Nuclear Instruments and Methods in Physics Research A294 (1990) 446–458
North-Holland

A HIGH-RESOLUTION LEAD/SCINTILLATING FIBER ELECTROMAGNETIC CALORIMETER

D.W. HERTZOG, P.T. DEBEVEC, R.A. EISENSTEIN, M.A. GRAHAM, S.A. HUGHES, P.E. REIMER and R.L. TAYLOE

Department of Physics and Nuclear Physics Laboratory, University of Illinois at Urbana-Champaign, Urbana, IL 61801, USA

Received 20 March 1990

Electromagnetic calorimeter modules based on a uniform array of plastic scintillating fibers embedded in a lead alloy have been built and tested. Techniques have been developed to assemble large volumes of this composite material and to machine it into the tapered trapezoidal modules appropriate for modern, hermetically-sealed calorimeters with pointing geometry. Using this technique, a 300-element array of such modules has been built and instrumented. Prototypes and subsets of the larger array have been tested in electron and photon beams ranging in energy from 0.035 to 5.0 GeV. Improvements in fiber characteristics, assembly procedures, and geometrical optimization have led to substantial performance gains over previous similar detectors. The average resolution of these detectors is determined to be $\sigma/E \approx 6.3\%/\sqrt{E}$ (GeV). The techniques of fabrication and the detector tests are described.

1. Introduction

Our group is designing and building the electromagnetic calorimeter (EMC) belonging to the multipurpose JETSET [1] detector which will be operated at the CERN Low-Energy Antiproton Ring (LEAR). The detector has cylindrical geometry and consists of forward and barrel regions. It surrounds a molecular hydrogen cluster jet target which intersects the circulating antiproton beam in LEAR. The EMC must satisfy four design criteria: it must have good position and energy resolution for reconstruction of π^0 and η mesons; it must be fairly dense due to limitations in the size of detector envelopes; it must have a low energy threshold for alternate use as a gamma veto from low-energy π^0 decay; and it must have a fast response time (< 100 ns) for use in the first-level trigger scheme. These criteria are satisfied by an EMC made of individual towers with photomultiplier tube readout. The towers point to the interaction region and from a hermetically sealed structure. They are required to be tapered trapezoids in both the barrel and forward detectors. The design depth is 12.5 radiation lengths (X_0).

Such towers could be made from existing technologies, such as lead glass or any of the inorganic crystals (BGO, CsI, NaI, BaF). However, such options are quite expensive. We felt that many of the excellent features of these choices could be maintained, but at a cost more typical of lead/scintillating-plate sandwich structures, if an improved version of the lead/scintillating fiber (Pb/SCIFI) technique [2–5] could be developed. The results of our development program are the subject of this paper.

Early successes with the project [6] have led to the final design, construction and installation of the 300-element JETSET forward calorimeter. An array of nine of these modules has been tested in a monoenergetic electron beam at CERN and 240 elements of the array were used in an experiment [7] at LEAR. All of the detectors studied in dedicated test beam environments have exhibited excellent resolution.

2. Design considerations

The Pb/SCIFI calorimeter blocks consist of a matrix of 1 mm diameter clad, polystyrene-based scintillating fibers embedded in a lead alloy (fig. 1). All fibers are aligned in parallel when the block is constructed. This block is then machined to a tapered trapezoidal shape (a tower) which is oriented such that the fibers point toward the interaction region. This enables direct light collection on the rear face of the tower. Dead spaces due to conventional wavelength shifter bars in sandwich designs are avoided. In practice, the normal with respect to the tower face must be tilted by a few degrees with respect to incoming photons to ensure that all incident trajectories from the target region encounter the lead and not only the scintillator. The volume ratio of fiber-to-lead affects both the energy resolution and the equality between the response to the electromagnetic and hadronic components of showers (e/h ratio). These responses cannot be simultaneously optimized. While energy resolution improves with increasing fiber content, an e/h ratio of unity is expected [8] when the ratio of fiber-to-lead is approximately 1 : 4.

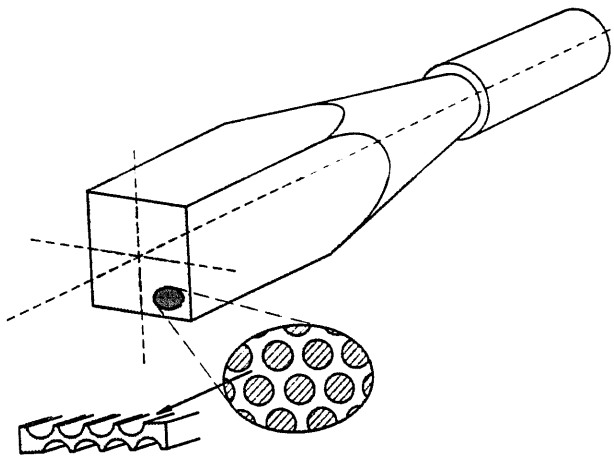

Fig. 1. A Pb/SCIFI detector including the lightguide and photomultiplier tube arrangement. The insets indicate the relative spacing of the scintillating fibers and a profiled lead plate from which the basic construction is derived.

The advantages of fiber calorimeters have been well documented [2–6]. Such detectors are:

- dense (radiation length of 0.8 to 1.6 cm depending on fiber-to-lead ratio),
- fast (same as plastic scintillator when read out with photomultiplier tubes),
- radiation resistant (characteristic of polystyrene, exceeding 10^6 rad),
- capable of good position resolution from energy sharing among towers,
- relatively inexpensive (similar to that of lead/scintillator sandwich geometries),
- capable of providing good hermeticity and uniformity of response.

Previous groups which pioneered this technique have built the Omega inner calorimeter (OIC) [2] and the DELPHI-Bergen small-angle tagger (SAT) [9]. In each of these detectors the approximate volume ratio of fiber-to-lead was 1:1 leading to a radiation length of approximately 1.1 cm. While the SAT is assembled from alternating strips of fiber ribbons and flat lead sheets, the OIC required that the fibers be positioned uniformly throughout the lead with alternating fiber rows being offset by half a fiber spacing. This has the advantage of finer sampling and thus better energy resolution (section 5).

We chose to modify this design slightly by making our fiber-to-lead ratio 50:35, leaving 15% volume for filling around the fibers with an epoxy. The density of a finished block is found to be $\rho_{Pb/SCIFI} = 4.58$ g/cm^3 leading to a radiation length in our design of $X_0 = 1.61$ cm. The fibers are placed exactly on the corners of equilateral triangles with a fiber-to-fiber spacing of 1.35 mm (fig. 1). The tapered trapezoidal tower is achieved by first building full rectangular blocks with fibers running along the length of the block and afterwards machining the four long sides to the appropriate form. In our design, because of the machined taper angle, approximately 70% of the fibers extend completely from the front to the back of the tower. Since light is collected only on the back face (no mirrored front face), no particular adverse effect from the taper, other than a

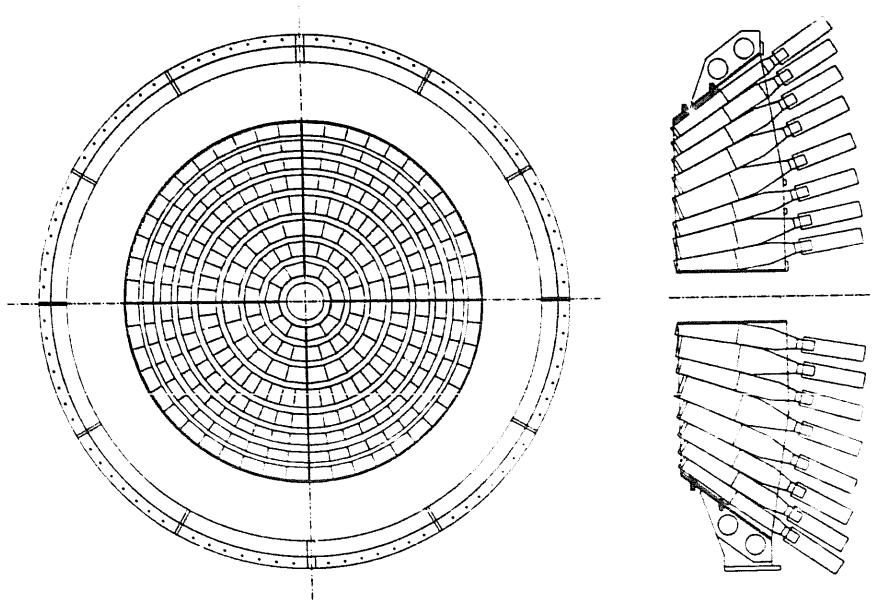

Fig. 2. Front and side views of the 300-element forward calorimeter including a part of the mechanical support system. Each tower is pointing to a position along the beam axis, 80 cm upstream. The actual interaction point in the JETSET experiment is 61 cm upstream. The side view illustrates the pointing geometry, assembly cradle, and overall length of the detectors.

thin inactive layer of about one fiber thickness on each side face, was expected or seen.

The JETSET forward calorimeter (fig. 2) requires 300 towers in 38 different shapes which are assembled into eight concentric rings around the beam axis. These rings contain 12, 24, or 48 towers and are interrupted only at the vertical and horizontal axes by thin steel supports. Otherwise, each quarter of the forward calorimeter is hermetically sealed. The mechanical support splits the calorimeter into two symmetric sections along a vertical line centered on the beam axis. These sections can be readily installed and removed as individual units.

Each of the EMC towers is 20 cm in length and has nearly constant front and rear surface areas of 36 and 53 cm^2, respectively, in the shape of a trapezoid. With the circumference of the rings increasing for larger polar angles, both the height and width of the towers are varied to maintain these constant areas. The towers are machined to their proper shape from rectangular blocks of different sizes, each corresponding to one of the rings in the system.

A conically-shaped acrylic lightguide is glued to the rear face of each tower with the trapezoidal shape of the rear face of the tower being cut into the guide. The overall length of the lightguide is 25 cm and includes a 5 cm long straight cylindrical section which is coupled to either a Philips XP2072 or an EMI 9902 photomultiplier tube (PMT). An aluminium collar is mounted around this straight section and is used to support the PMT and base assembly. In addition, it is used as a part of the overall support and positioning fixtures of the towers within the calorimeter frame. A complete module (tower, lightguide, and phototube) is shown in fig. 1, and a front and side view of the forward calorimeter array is shown in fig. 2.

3. Pb/SCIFI tower construction

The first step in the assembly of the basic element, the Pb/SCIFI block, is to produce lead alloy plates with the profile shown in the inset of fig. 1. A custom rolling machine has been developed [10] to form these from 0.46 mm thick, flat sheets cut from bulk rolls of the lead alloy. The machine includes a negatively-profiled steel die which is pushed under the surface of an oppositely-keyed cylindrical steel drum. A flat sheet, whose cross-sectional area nearly equals that of the finished profiled plate, is placed on top of the bottom die, which is then pushed by a hydraulic cylinder under the freely rotating cylindrical drum. The drum is fixed in height above the bottom die set. A single back and forth stroke has been found to produce consistently uniform, flat, and properly grooved plates. The machine is a self-contained unit capable of producing the tens of thousands of plates which are required for the calorimeter blocks. Each profiled plate can be made in less than one minute. Auxiliary tools have been made to trim the ends of the plates to length without crushing the de-

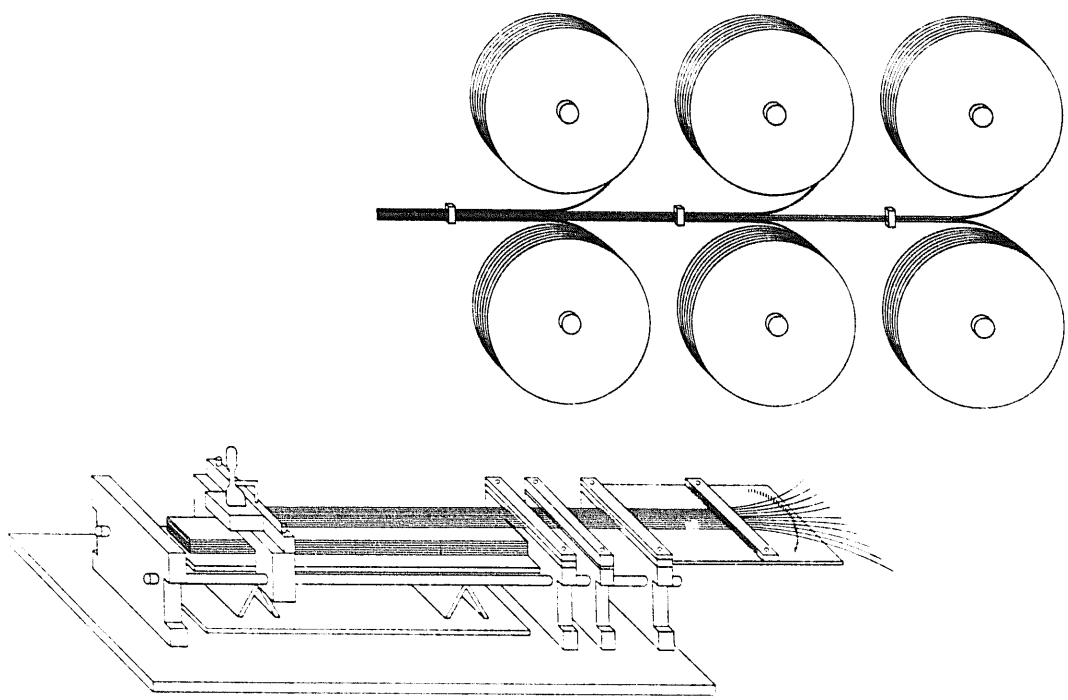

Fig. 3. Illustration of the assembly process (not to scale) including the arrangement of the fiber spools and the relevant features of the weaving machine.

licate profile and to prepare custom-width plates which are required for the construction of the different rectangular shapes.

The metal used is an alloy of lead (Pb) containing 6% antimony (Sb) by weight. This has far superior mechanical properties compared to pure Pb. In particular, pure Pb tends to stick to the die surface, to bend when removed, and to deform easily when handled. The stiffness that results from the introduction of a small amount of Sb is essential since the profiled plates must be very flat to keep the fibers inside the grooves during assembly. Once profiled, the plates contain a residual amount of machine oil which is removed after a 4-min immersion in an ultrasonic bath.

The scintillating fibers are type S101-S produced by Optectron [11]. They are delivered on 75 cm diameter spools, each containing 400–600 m of material. A weaving machine (fig. 3) which was built at our laboratory can be loaded with up to 72 of these spools at one time. The machine includes a guiding system that brings the fibers along parallel paths, each fiber being spaced 1.35 mm from its neighbor. This corresponds to the groove spacing of the profiled lead plates. An assembly station is located downstream of the fiber guides and includes a table with vertical travel upon which alternate layers of fibers and profiled plates are stacked; the guided fibers are kept at a constant elevation. A clamp, mounted to a rail system, is used to clasp uniformly the ends of all of the fibers and draw them, maintaining their straightness and relative alignment, across the assembly table. In practice, four of the detectors are built at once, end to end.

A smooth layer of optical epoxy (having a low viscosity and relatively long work time [12]) is applied to the top of each lead plate before each layer of fibers is strung, and then to the top of those fibers before the next lead plate is stacked. The epoxy envelops each fiber. This is found to be necessary for machining of the finished blocks without dislocation of the fibers or separation of the plates. We have observed no adverse effect on the fiber due to the use of this epoxy. One of the earliest prototypes has been repeatedly tested periodically over 1.5 years, and its performance is unvarying.

After 48 h of drying time under pressure, the long Pb/SCIFI bar created in the assembly procedure is divided into four separate blocks. One side of each block is machined to a flat surface, parallel to the orientation of the fibers, on which final machining of the tapers can be based. This last step is done on numerically controlled machines to ensure excellent reproducibility in reasonable time.

The total assembly time for the four-block bar averages approximately 11 h. For each assembly hour, an additional hour is spent on the preparation and cleaning of the lead plates, the maintenance and reloading of the weaving machine, and preparation of the epoxy. A finished tapered tower can be derived from a rectangular block in less than two hours of milling-machine time.

After milling, the ends of the block are polished and a lightguide is glued to the block using the same optical epoxy as in the assembly process. An ultraviolet transmitting plastic prism is attached to the front face of the detectors for eventual connection to a N_2 laser (337 nm) light-distribution system, which is being developed as a relative calibration system for the EMC in the JETSET experiment. The lightguide is wrapped in Al foil and the detector–lightguide combination is then covered with two layers of 0.15 mm thick, black PVC heat-shrinkable tubing [13] in order to light-seal the entire assembly.

4. Test runs and results

A number of prototype detectors have been built and tested. However, the results of general interest come mainly from a $10 \times 10 \times 22$ cm^3 ($14X_0$ depth) untapered prototype and from an array of nine tapered towers which are a part of the final forward calorimeter. The former, whose lateral dimensions were chosen for full shower containment, was used to test under nearly ideal conditions the resolution, light output, and long-term reliability of our implementation of the Pb/SCIFI technique. The array was used to observe how such properties might change in a situation in which energy was distributed over several towers. Problems of interest included light output uniformity among the towers and across the tower boundaries. Additionally, the array was used to study impact position resolution.

The prototype detector was tested using monoenergetic electron and tagged-photon beams at the University of Illinois microtron ($E_{e^-,\gamma} < 0.1$ GeV), the T11 pion/electron test beam at the CERN-PS (0.3 GeV < $E_{e^-} < 1.5$ GeV), and an electron beam at DESY (1.0 GeV < $E_{e^-} < 5.0$ GeV). The array of nine towers was tested only at the T11 area, and was subsequently used as a part of the full calorimeter array in the PS185 experiment [7] at LEAR. In all cases, a charged-particle beam was defined by a set of plastic scintillation trigger counters arranged to provide a well-defined impact position on the front face of the detectors. At the T11 test beam, a N_2 gas Cherenkov counter was used to select electrons in a beam which also contained negative pions. For each event, the integrated charge from the photomultiplier tubes was measured and recorded on magnetic tape along with trigger information.

4.1. Tests with an indiviaual detector

The prototype detector was coupled to a Burle Industries 8850 Quantacon photomultiplier tube [14] with

a solid acrylic lightguide of total length 30 cm. The lightguide matched the rear square face of the Pb/SCIFI block and was tapered conically to a diameter of 4.5 cm, matching the PMT photocathode.

The PMT–ADC system was calibrated in channels per photoelectron (pe) immediately prior to one of the test runs by the following procedure. Electrons from a collimated ^{106}Ru source were constrained to pass through a thin trigger scintillator before entering the front face of the Pb/SCIFI module. A signal from this trigger counter was used to gate the ADC as the beam trigger counters do during the actual tests with higher-energy electrons. The Quantacon PMT incorporates a gallium-phosphide first dynode to give a distinct single photoelectron signal. A gain of 6 channels per pe was observed at an operating voltage of −2200 V. With no changes in the setup, the calorimeter module was tested using a 0.093 GeV electron beam. The mean of the resulting peak corresponded to 90 pe, or 970 pe/GeV. This figure *includes* light losses in the lightguide system and losses due to attenuation in the fibers.

Photons entering the lightguide come from approximately 6300 evenly spaced individual fibers. For a lightguide with an adiabatic reduction in cross-sectional area, the transmission efficiency (ϵ_{LG}) of the lightguide is equal to the ratio of the exit to the entrance areas [15]. For the Pb/SCIFI prototype this gives $\epsilon_{LG} = 0.16$. However, since the light from the fibers enters the lightguide in a relatively narrow forward cone, ϵ_{LG} will be larger. The angle of emitted light from any individual fiber with respect to the fiber axis is limited by the ratio of indices of refraction of the fiber core to its cladding, with

$$\theta_{\text{fiber}} \leqslant \arccos\left(\frac{n_{\text{cladding}}}{n_{\text{core}}}\right)$$

leading to a maximum half-angle of $\theta_{\text{fiber}} = 29°$. The same calculation for the acrylic lightguides with an air interface leads to a maximum half-angle of $\theta_{\text{guide}} = 48°$. Conservation of phase space implies that the ratio of photocathode area to Pb/SCIFI block face need only be $(\sin\theta_{\text{fibers}}/\sin\theta_{\text{guide}})^2 = 0.43$ to collect all of the photons emitted from the fibers [5,15]. Since the lightguide employed in our system has a ratio of exit to entrance areas smaller than 0.43, we expect to transmit approximately $\epsilon_{LG} = 0.16/0.43 = 0.37$, in the limit of an infinitely-long tapered guide. We have performed ray-trace simultaneous [16] of the transmission efficiency through a perfect-surface, conical lightguide as a function of the exit to entrance area ratio, and find agreement with the above model in the limit of a very long lightguide.

The behavior of the energy resolution (σ/E) versus energy is shown in fig. 4 for the prototype detector over a wide range of energies. The dotted line through the energy resolution data follows a $1/\sqrt{E}$ power law as

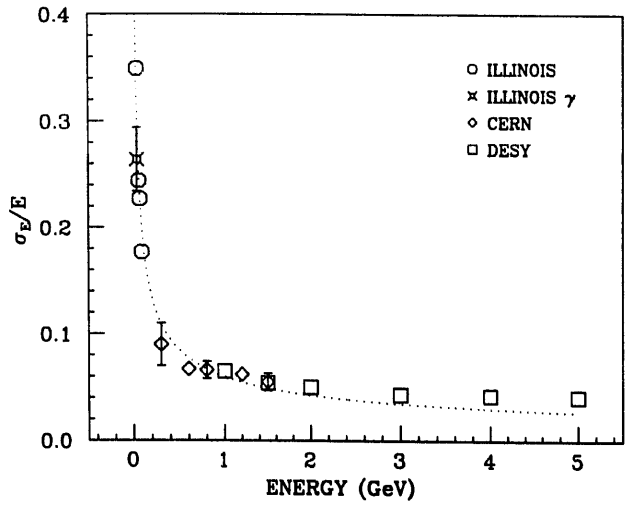

Fig. 4. Resolution (σ/E) versus energy for a single large prototype Pb/SCIFI detector. The solid line falls as $1/\sqrt{E}$ consistent with that expected from a detector dominated by sampling fluctuations. The data point at 0.045 GeV was obtained using monoenergetic photons, while the rest of the data used incident electrons.

expected for a detector whose resolution is principally determined by sampling fluctuations. Hereafter, we quote the resolution of the detectors as

$$\frac{\sigma(E)}{E} = \frac{X}{\sqrt{E}}$$

with E in GeV. The OIC [2] and SAT [9] Pb/SCIFI detectors have reported resolution figures of $X = 10.0\%$ and 10.9%, respectively, for similar designs. The value of X corresponding to the line drawn in the figure is 6.0%. The deviation of the data from the line at the highest energies is largely due to energy leakage.

If Pb/SCIFI blocks are positioned within a calorimeter such that fibers point directly to the interaction region, then it is possible for the modules to look partially transparent to energetic photons. In the CERN OIC, this was avoided by deforming the blocks slightly with a wavy structure so that no fiber was exactly straight. Fearing that the mechanical stress placed on the fibers by this technique might damage the fibers or crack the cladding, we studied the performance of the detector as a function of incident angle of the beam in order to choose, instead, an appropriate tilt angle for all of the towers. A plot of the resolution versus angle for the prototype is shown in fig. 5 where an incident 0.088 GeV electron beam with negligible divergence was used. A slight deterioration in the resolution is realized as parallel incidence is approached, where we expect a greater degree of longitudinal fluctuations to influence the performance. The situation may be worse for photons since the location of the first interaction may be quite deep into a block for a photon trajectory inside and nearly parallel to a plastic fiber.

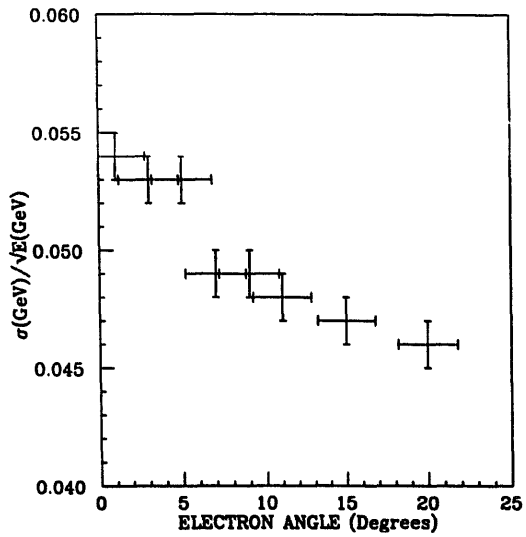

Fig. 5. Resolution in $\sigma/E = X(\%)/\sqrt{E}$ versus angle of the prototype for an incident 0.088 GeV electron beam. A slight rise in resolution is observed near parallel incidence. Note the zero-suppressed scale on the ordinate.

4.2. Energy resolution of a small array

A subset of the forward calorimeter consisting of nine towers was tested in the CERN T11 beam using electrons and negative pions in the range of 0.3–1.2 GeV/c. The orientation of the detectors with respect to the beam is shown in fig. 6a along with the coordinate system used in the calculation of positions. The location of the beam impact points [A–F] which were used in the impact-position analysis are given in the figure. The corresponding orientation within the actual calorimeter is indicated in fig. 6b. The towers which make up the array of nine are enclosed in a dotted box. The tilt angle between the beam and the center line of the central block is 5.6° and the beam is always maintained parallel to the line shown in fig. 6b. As a result, the tilt angle in the tests varied from 1.8° to 10.4°; in the actual calorimeter, the range is 6.3° to 5.0°, for the same towers, respectively.

The relative calibration of seven of the nine towers was achieved by requiring the position of the minimum ionizing pion peak in the ADC spectrum of each block to be the same. A typical distribution at 0.8 GeV/c which includes both the pion and electron peaks for the central tower is shown in fig. 7b. With the Cherenkov detector in the trigger, only the higher-energy electron peak is visible (fig. 7a). Due to time limitations, two of the towers were only approximately calibrated using an extrapolation based on the pion calibration method described above. In those cases the data were obtained at different high-voltage settings than those finally used in the dedicated electron runs.

In contrast to the prototype detector, no individual tower in the array of nine was sufficient to contain the

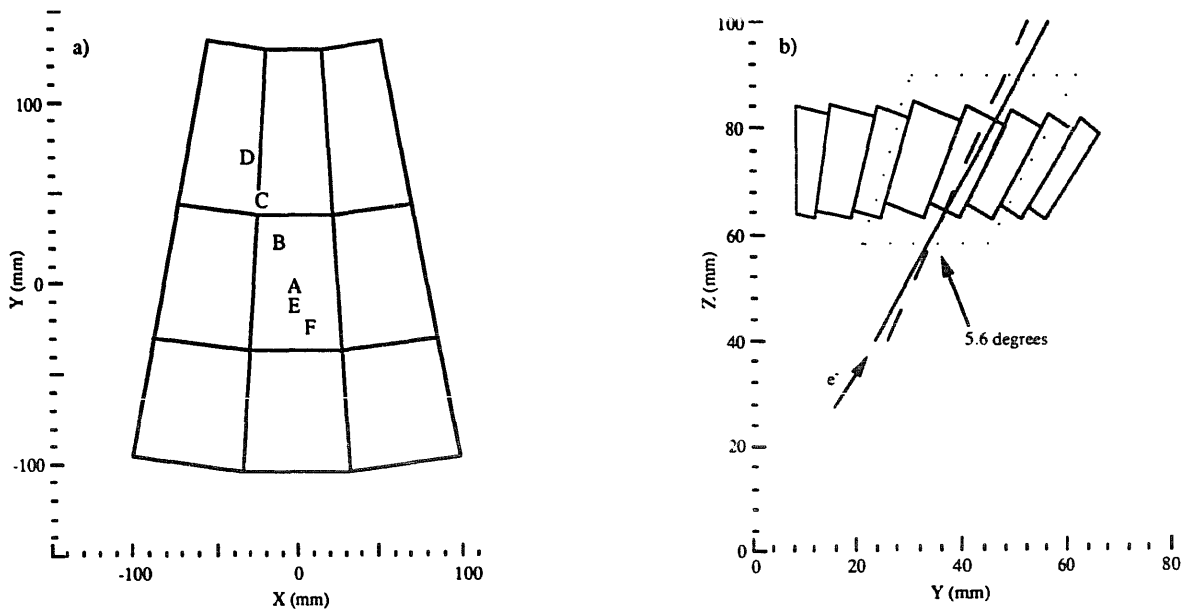

Fig. 6. (a) View, looking downstream, of the front faces of the array of nine towers including the coordinate axis used in the position analysis and the impact points of the six runs [A–F]. (b) Side view of the geometry of the towers in the JETSET forward calorimeter configuration (fig. 2). Note that the angle of the beam with respect to the fiber axis is slightly different in the test runs as compared to the actual JETSET geometry. The dotted box encloses the tested towers.

lateral spread of a shower. Consequently, the balanced energy sum, defined as

$$\text{balanced sum} = \sum_{i=1}^{9} (\text{calibrated ADC})_i,$$

was used in calculations of the energy resolution of the system. A Gaussian function gave an adequate description of the balanced sum peak shape, and a fitting procedure, applied over an energy window of approximately $\pm 3\sigma$ from the peak, was used to determine the actual centroid and width. Figs. 8a and 8b show the energy dependence of the balanced sum centroid and resolution with the beam impact position in the center of the central tower. The errors on the resolution are due to both the fitting routine and the conversion of channels to energy. The momentum spread of the beam has been subtracted in quadrature assuming $\delta P/P =$ $(1.5 \pm 0.5)\%$ according to the quoted momentum resolution of the beam. Note that the performance of the array, as indicated by the excellent resolution figure $\sigma/E = 6.3\%/\sqrt{E}$, does not differ substantially from what was found under ideal conditions with the prototype. At the relatively low energies at which these detectors have been tested, no constant term is needed in the description of $\sigma(E)$.

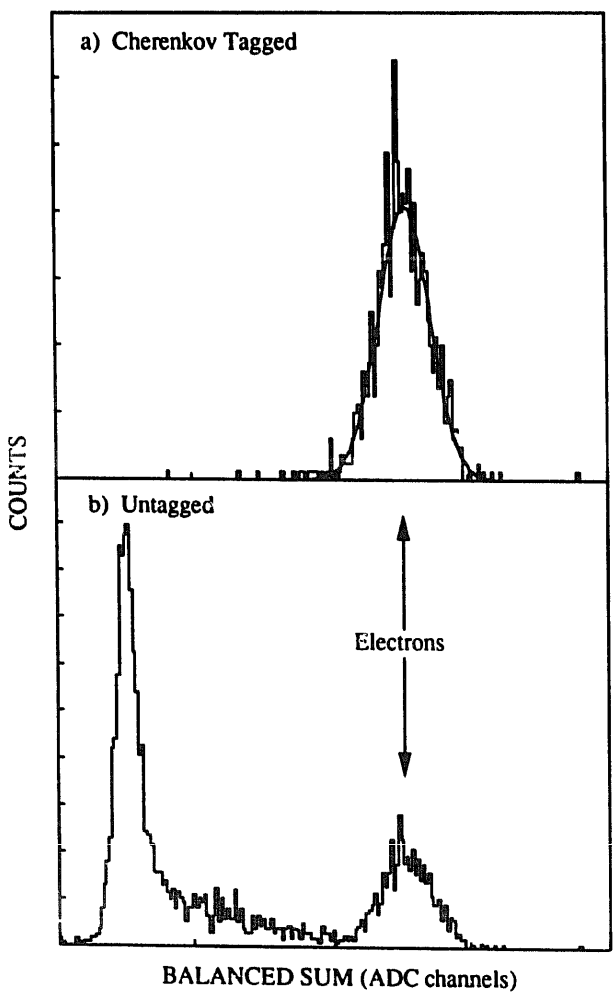

Fig. 7. Typical response of a Pb/SCIFI tower to the T11 test beam at 0.8 GeV/c. The peak on the left in (b) is due to minimum ionizing negative pions which travel the length of a tower. This peak is used for a tower-to-tower relative calibration. The peak on the right is due to electrons as illustrated more clearly with the Cherenkov condition (a) in the trigger.

A more stringent test involves the behavior of these same two quantities as a function of position from the center of the array. Figs. 9a and 9b indicate the centroid of the balanced sum and the energy resolution versus radius of the impact position for a 0.8 GeV incident electron beam. The fluctuations of the results about the respective averages are within the errors of the measurements. Positions [C] and [D] are sufficiently far from the center of the array such that energy leakage of the balanced sum begins to enter. No neighbor towers exist in the upper left corner of the array (fig. 6a).

The Molière radius of these detectors, based on a simple calculation [17], is 3.5 cm. The measured ratio of the mean of the central tower's energy distribution to that of the balanced sum is plotted as a function of incident energy in fig. 10. The dashed line indicates about 90% of the contained energy is deposited in the center tower alone. The radius of 90% containment corresponds to roughly one Molière radius for a $12.5X_0$ detector [18]. If an effective radius is defined as the radius of the circle whose area is the cross-sectional area of the block, then the effective radius varies from 3.4 to 4.1 cm as a function of the depth of the tapered tower.

The relative size of a 1 GeV, photon-induced, electromagnetic shower can also be seen in fig. 11. Here, a Monte Carlo simulation [19] was used to track the energy deposition laterally (fig. 11a) and longitudinally (fig. 11d). In figs. 11b and 11c, the projections of energy deposition versus radius and depth are also shown. These figures are provided to illustrate the extent of the shower size in these detectors which in turn governs the tower segmentation size.

4.3. Position resolution of a small array

An estimate of the beam impact position can be obtained by calculating

$$\bar{x} = \frac{\sum_{i=1}^{9} x_i E_i^{\alpha_x}}{\sum_{i=1}^{9} E_i^{\alpha_x}} \quad \text{and} \quad \bar{y} = \frac{\sum_{i=1}^{9} y_i E_i^{\alpha_y}}{\sum_{i=1}^{9} E_i^{\alpha_y}}, \tag{1}$$

where x_i, y_i and E_i are the coordinates and energy deposited, respectively, in the ith tower, and α is a parameter used to weight the importance of the contributions [20]. For example, $\alpha < 1$ emphasizes the importance of the energy deposited in the periphery of the

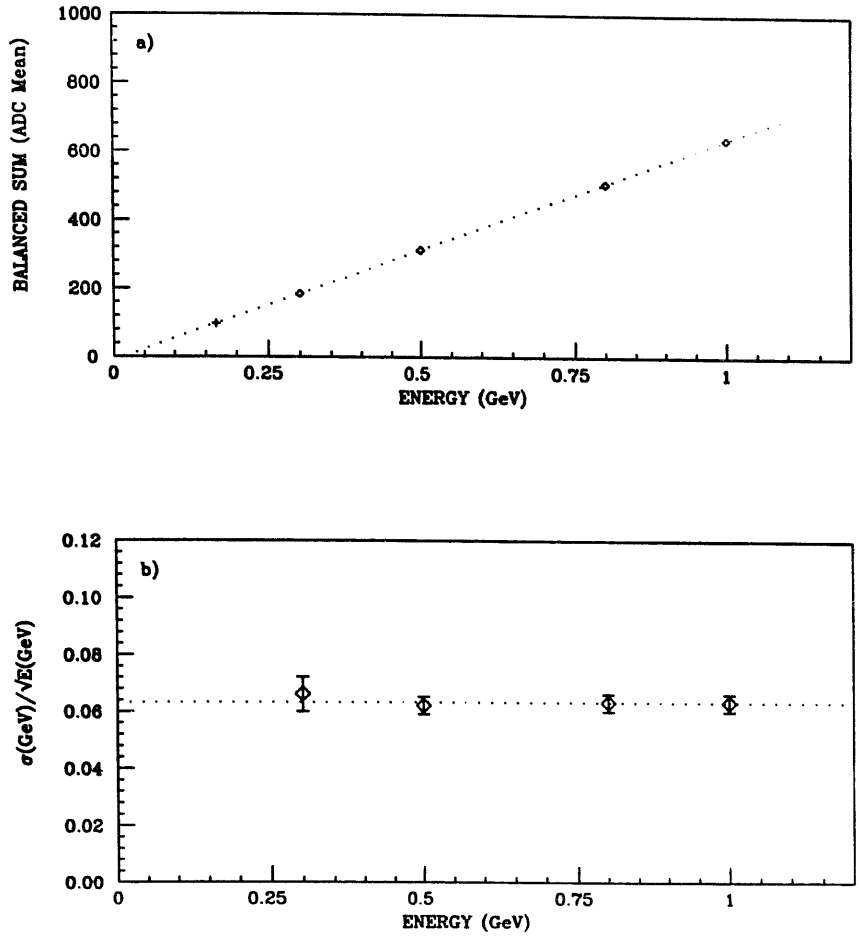

Fig. 8. (a) Total energy in the array of nine towers versus energy and (b) energy resolution of the sum versus energy. These data were obtained with the beam incident in the center of the central tower. The dotted line in (b) represents a resolution of $\sigma/E = 6.3\%/\sqrt{E}$.

shower. Six runs at a fixed beam energy of 0.8 GeV were made at the different positions [A–F] indicated in fig. 6a. We used an iterative procedure to optimize α_x and α_y. For each beam position and a given value of α_x and α_y, the distributions $\bar{x}$ and $\bar{y}$ were obtained using eq. (1). The distributions are generally asymmetric for an α chosen near 1 and approach true Gaussians as α is decreased. The α dependence of the weighted average position error is shown in fig. 12. A clearly visible minimum is realized at values of α_x and α_y equal to 0.68 and 0.59, respectively. Using these parameters, the difference between the calculated and real impact positions is compared to the real position. The comparison is shown in fig. 13. In practice, the real position is a measured offset with respect to position [A]. The error bars in fig. 13 include the finite size of the beam impact position which can be removed by the procedure outlined next.

The beam profile on the front face of the detector was defined by a square trigger scintillator with sides a equal to 10 mm. Assuming that a Gaussian function of width σ^G describes the resultant position distribution for the case of a pointlike beam incident on the detector, then the measured position distribution should be given by the convolution of the square beam profile with the Gaussian response

$$F(x) = \int_{-\infty}^{+\infty} s(u)g(x, u)\,du,$$

where

$$s(u) = \frac{1}{a} \qquad -\frac{a}{2} \leqslant u \leqslant \frac{a}{2};$$

$$s(u) = 0 \quad \text{otherwise},$$

and

$$g(x, u) = \sqrt{\frac{1}{2\pi(\sigma^G)^2}}\exp\left(\frac{-(x-\mu)^2}{2(\sigma^G)^2}\right).$$

Integrating, we find

$$F(x) = \frac{1}{2a}\mathrm{erf}\left(\frac{\frac{a}{2}-x}{\sqrt{2}\,\sigma^G}\right) + \frac{1}{2a}\mathrm{erf}\left(\frac{\frac{a}{2}+x}{\sqrt{2}\,\sigma^G}\right).$$

The measured convoluted width was found to be σ_x^{convul}

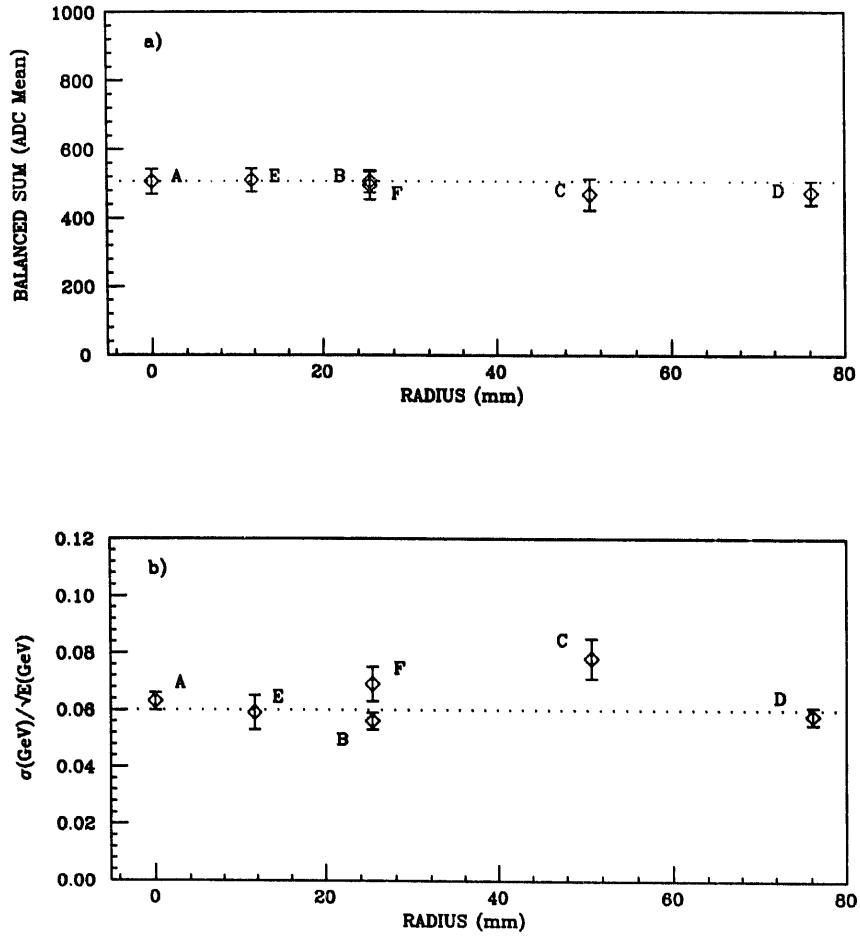

Fig. 9. (a) Total energy in the array of nine towers versus distance from the center of the array. The individual runs [A–F] are also indicated on the plot and correspond to the labels in fig. 6a. The dotted line is centered at point [A]. Error bars represent the width of the peak. (b) Energy resolution of the sum versus distance from the center of the array. These data were obtained with a 0.8 GeV incident electron beam. The dotted line represents the average.

$= (4.5 \pm 1.6)$ mm and $\sigma_y^{\text{convul}} = (7.9 \pm 2.6)$ mm, which leads to an implied position resolution (square beam profile removed) of $\sigma_x^{\text{G}} = (3.0 \pm 1.6)$ mm and $\sigma_y^{\text{G}} = (7.5 \pm 2.6)$ mm. The y dimensions exceed the x dimensions (63 vs 53 mm) for the towers used in the measurements. This leads to a smaller degree of energy sharing verti-

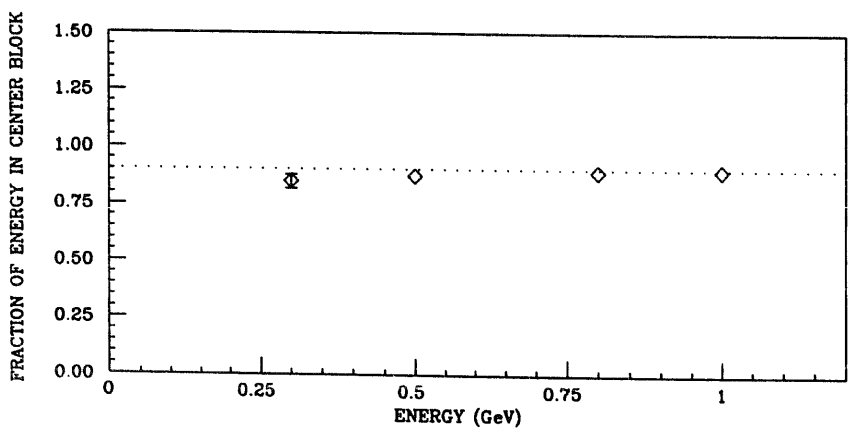

Fig. 10. The ratio of energy deposited in the central tower compared to the total contained energy (the balanced sum). The dotted line indicates that an individual tower contains approximately 90% of the energy of a shower incident at its center.

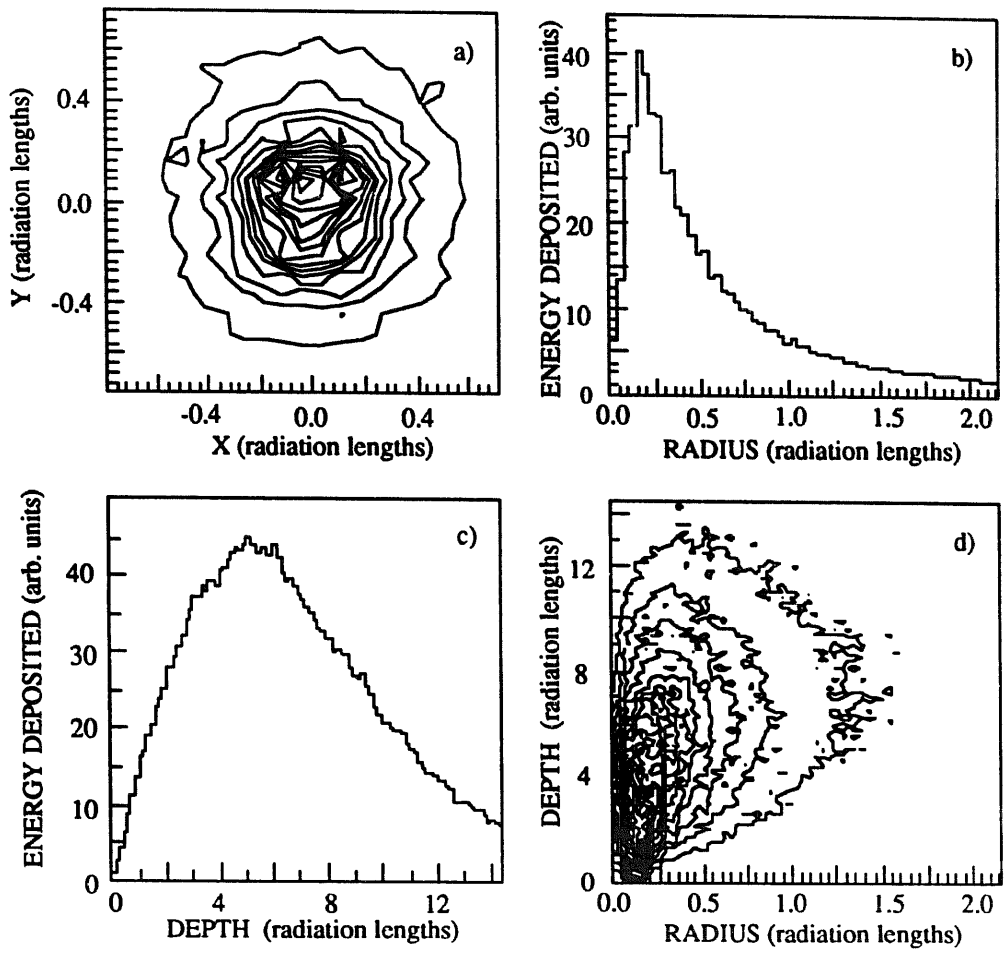

Fig. 11. (a) A contour plot of the energy deposited (beam view) in a Pb/SCIFI detector from Monte Carlo simulations using 1 GeV incident photons. (d) The same distribution versus depth and radius. Projections of the energy deposition versus (b) radius and (c) depth are also shown. These scales are in radiation lengths with $X_0 = 1.61$ cm for the detectors described here.

cally compared to horizontally. Additionally, the beam was incident on the towers at a larger angle in the y direction than in the x direction. These considerations are partially responsible for $\sigma_y > \sigma_x$.

While these tests were all made at a fixed beam energy, the actual behavior of the position resolution is expected to follow a $1/\sqrt{E}$ law similar to that of the energy resolution. The position resolution at point [A]

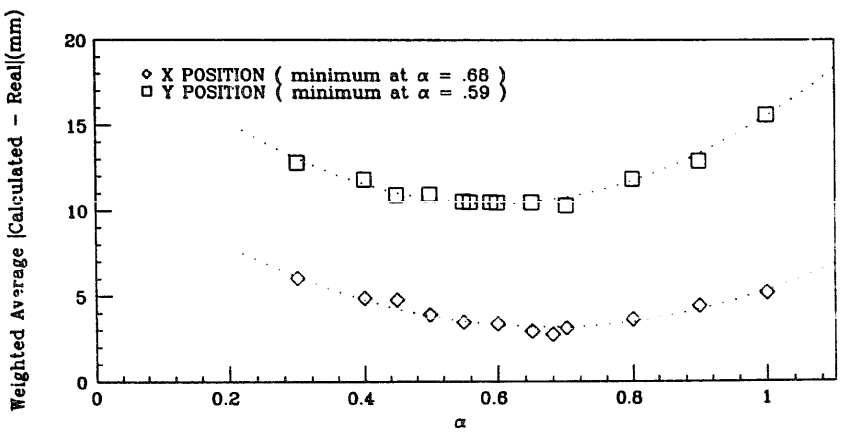

Fig. 12. The width, determined by a Gaussian fit, of the position distributions for x and y versus different weighting constants, α_x and α_y. Minima are observed at $\alpha_x = 0.68$ and $\alpha_y = 0.59$.

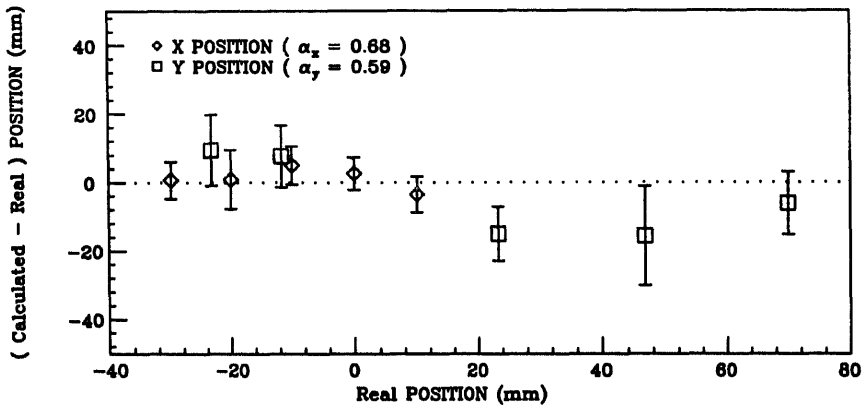

Fig. 13. The difference between the calculated and real impact position versus the actual position with respect to the origin of the array of nine towers. The error bars for each point include the uncertainty due to the finite size of the incident beam.

was checked for this behavior using the energy scan data and follows this trend, as shown in fig. 14.

4.4. π^0 mass resolution with a large array

An array of 240 Pb/SCIFI towers (rings 5–8, fig. 2) was used to detect the photon from the decay $\Sigma^0 \rightarrow \gamma\Lambda$ in experiment PS185 at LEAR [7]. Relative calibration data was obtained using a trigger which enhanced the probability for one and only one minimum ionizing particle to pass through a single tower. The centroids of the resulting distributions were normalized and an energy scale was established for each tower. A second trigger, $\bar{p}p \rightarrow$ neutrals, was used for an absolute energy calibration based on reconstruction of a π^0 from two observed photons inside the array. In a preliminary analysis of this data, a clear peak in the invariant mass spectrum of the two photons, centered at the π^0 mass, is observed as shown in fig. 15. The width of this peak is $\sigma/M_{\pi^0} \approx 0.11$. The momentum distribution of the π^0s in this sample varies from 0.3 to 2.4 GeV/c.

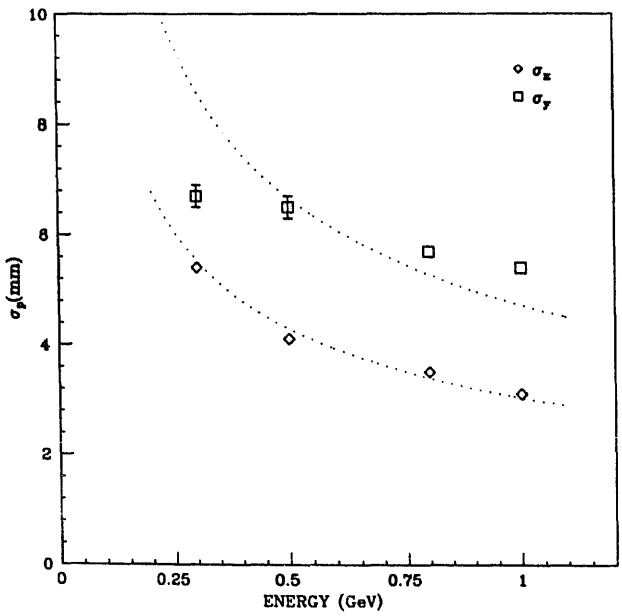

Fig. 14. The position resolution versus energy for the data obtained at point [A]. A $1/\sqrt{E}$ curve is drawn through the points indicating the expected improvement in position determination as the statistics in the shower sampling are increased.

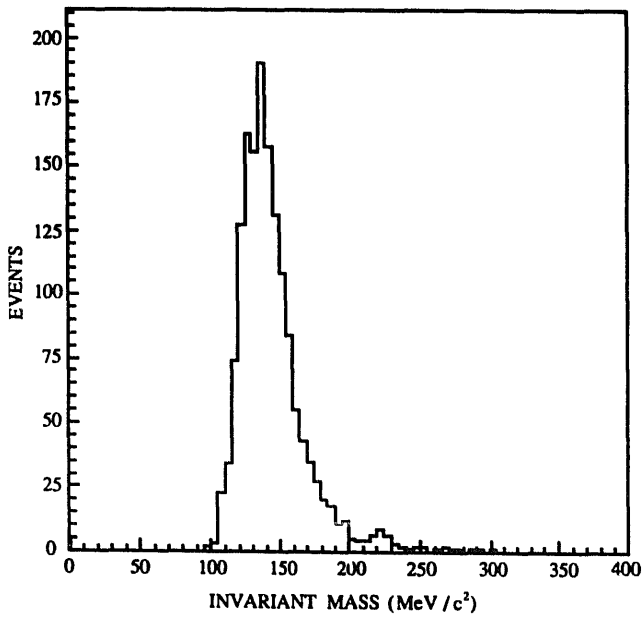

Fig. 15. Invariant mass from reconstruction of two photon clusters in an array of 240 Pb/SCIFI towers. The peak is centered at the π^0 mass.

5. Simulations with other geometries

The Monte Carlo program GEANT [19] is being used to describe the exact geometry of the Pb/SCIFI

detectors and to model the deposition of energy inside the active and inactive components of these detectors for electromagnetic showers. To the extent that the simulation program is accurate, the theoretical detector resolution, shower profiles, and possible geometrical changes for alternate, but similar, detectors can be studied. The advantage of using GEANT is that it is possible to describe exactly the complex geometry of the fibers as they are configured in the lead blocks.

While the detectors described here (the "reference" detectors) yield quite satisfactory results, alternate designs might be optimal in other applications where speed of construction, costs, or resolution demands differ from those we faced. A comparison of expected energy resolution with respect to the reference detectors has been made for three alternative geometries. In all cases the comparison is made using 1000 simulated 200 MeV photon showers incident at 3° with respect to the fiber axis. The results are quoted as $\sigma_{\text{alternate}}/\sigma_{\text{reference}}$.

Ribbons with 1 mm square-sided and closely-spaced fibers are available commercially. A calorimeter can be envisioned in which stacks of alternating ribbons and flat lead foils are used, keeping the fibers aligned longitudinally as in the described reference geometry. A simulation of such a detector, maintaining the same ratio of fiber : lead : glue as in the reference detectors, yields $\sigma_{\text{ribbons}}/\sigma_{\text{reference}} = 1.15 \pm 0.05$. The less homogeneous sampling in the ribbon case compared to the equilateral distribution of the fibers in the reference geometry is responsible for the difference. In principle, the construction process for such a ribbon detector should be easier; however, the completed module is less stable to shear forces since there is no locking action of the plates with respect to the fibers and the neighboring layers.

The use of either 1.5 mm or 0.75 mm diameter fibers, preserving the ratio of fiber : lead : glue and using the equilateral placement geometry of the reference blocks, leads to a change in the number of fibers needed by factors of 0.44 and 1.8, respectively. The costs of the fibers, and partially the labor to install them, is driven mainly by the length of the fibers, rather than the volume. Therefore, the design choice must be weighed against both budget and performance needs. As expected, the coarser sampling of the larger fibers leads to a reduction in resolution, $\sigma_{\text{larger}}/\sigma_{\text{reference}} = 1.12 \pm 0.04$, while the finer sampling of the smaller fibers leads to a resolution improvement, $\sigma_{\text{smaller}}/\sigma_{\text{reference}} = 0.85 \pm 0.04$. If the material volume ratios are held constant, the number of charged-particle crossings (positrons and electrons traversing the active fibers) is inversely proportional to the fiber diameter. The statistical fluctuation on the number of such crossings in a given shower largely determines the detector resolution [21]. The simulation does not include the most relevant fiber performance characteristic, attenuation length. This may influence the eventual performance, particularly for the small-diameter fibers.

6. Conclusion

Electromagnetic calorimeter modules built using improvements in the Pb/SCIFI technique have been assembled and tested. The results from our resolution studies indicate that this technique now rivals the performance attainable from more expensive lead glass. The resolution of both the prototype and of the actual tapered towers is typically $\sigma/E = 6.3\%/\sqrt{E}$, which is a substantial improvement from that achieved previously with similar fiber-based calorimeters. The impact position resolution for the described tower geometry is typically 3.0–7.5 mm in x and y at 0.8 GeV. These figures partly depend on the sizes of towers used and the energy of the incident beam. A π^0 peak is clearly observed in an experiment employing a large array of such towers.

In addition to these fine performance characteristics, Pb/SCIFI detectors have the added benefits of being substantially more radiation resistant than lead glass and they have a shorter radiation length. Our group has built, installed and used a large array of Pb/SCIFI towers and has prepared several manufacturing tools in order to do this in a reliable, efficient, and consistent manner. No problems are envisioned in extending the dimensions of these blocks to suit other applications. With further improvements in manufacturing techniques and in fiber characteristics, we expect such detectors to become more common. Even at the present state of the technology, there are several clear advantages compared to both lead/scintillator-plate sandwich detectors and lead glass arrays.

Acknowledgements

The early design of this detector resulted from discussions with J. Kirkby and P. Sonderegger. Further design contributions were provided by R. Harfield and M. Price from the CERN EP TAG group. The fabrication of the detectors was made possible through the dedicated efforts of J. Gabbard, G. Garner, K. Gerlach, J. Ockers and, in particular, M. Moushmof. We were aided in the test runs reported here by R. Bock, M. Finn, R. von Frankenberg, B. Mouëllic, S. Ohlsson and members of the WA80 collaboration from the Universität Münster Group. This work was supported in part by the U.S. National Science Foundation under grant NSF PHY 86 10493.

References

[1] JETSET: Physics at LEAR with an Internal Gas Jet Target and an Advanced General Purpose Detector, Experiment PS202, CERN/PSCC 86-23, CERN, Freiburg, Genoa, Illinois, Jülich KFA, Oslo, Uppsala.

[2] P. Sonderegger, Nucl. Instr. and Meth. A257 (1987) 523.

[3] J. Kirkby, Today and Tomorrow for Scintillating Fibre (SCIFI) Detectors, CERN-EP/87-60 (1987), Proc. Workshop for the INFN Eloisatron Project: Vertex Detectors, Erice, Sicily, 1986, p. 225.

[4] H. Burmeister et al., Nucl. Instr. and Meth. 225 (1984) 530.

[5] H. Blumenfeld et al., Nucl. Instr. and Meth. 225 (1984) 518.

[6] D.W. Hertzog et al., Proc. Workshop on Scintillating Fiber Detector Development for the SSC, 1988, FNAL, p. 387.

[7] Study of Threshold Production of $\bar{p}p \rightarrow \bar{Y}Y$ at LEAR, Experiment PS185, CERN/PSCC/81-69, Carnegie-Mellon, Erlangen, Freiburg, Illinois, Jülich KFA, Uppsala, Vienna.

[8] J.E. Brau and T.A. Gabriel, Nucl. Instr. and Meth. A238 (1985) 489 and R. Wigmans, Nucl. Instr. and Meth. A256 (1988) 273.

[9] A. Klovning, Proc. Workshop on Scintillating Fiber Detector Development for the SSC, 1988, FNAL, p. 415.

[10] In conjunction with the Action Tool and Die Co., 3374 Precision Dr., Rockford, IL 61109, USA.

[11] Optectron, Z.A. Courtaboeuf, BP 535, Av. du Québec, F-91946 Les Ulis, France.

[12] Bicron Optical Cement BC-600.

[13] Manufactured by CMS Gilbreth Packaging Systems, 3300 State Rd., Bensalem, PA 19020, USA.

[14] Formerly RCA, New Products Division.

[15] Following R.L. Garwin, Rev. Sci. Instr. 23 (1952) 755.

[16] T. Massam, GUIDE 7 Reference manual, CERN 76-21.

[17] T. Yuda, Nucl. Instr. and Meth. 73 (1969) 301.

[18] See for example, C. Fabjan, in: Techniques and Concepts of High Energy Physics III, ed. T. Ferbel (Plenum, 1985).

[19] R. Brun et al., GEANT Reference manual, CERN DD/EE/84-1, Version 3.1305.

[20] R.L. Carrington et al., Nucl. Instr. and Meth. 163 (1979) 203.

[21] E. Amaldi, Phys. Scripta 23 (1981) 409.